Co-reactant Free Novel Self-enhanced Solid-state ECL Platform of Polyluminol-gold Nanocomposite for Highly Selective and Sensitive Signal-on Detection of Hg2+ ion

Venkateswara Raju Chikkili
1Electrodics and Electro Catalysis Division, CSIR-Central Electrochemical Research Institute (CECRI), Karaikudi - 630 003, Tamilnadu, India

Senthil Kumar Shanmugam (ssenthilmugam@gmail.com)
1Electrodics and Electro Catalysis Division, CSIR-Central Electrochemical Research Institute (CECRI), Karaikudi - 630 003, Tamilnadu, India

Research Article

Keywords: Self-enhanced solid-state ECL, Polyluminol-gold nanocomposite, Electrodeposition, co-reactant accelerators, Reactive oxygen species, Hg2+ sensor

Posted Date: December 10th, 2020

DOI: https://doi.org/10.21203/rs.3.rs-122366/v1

Version of Record: A version of this preprint was published at Scientific Reports on March 25th, 2021. See the published version at https://doi.org/10.1038/s41598-021-86195-1.

Abstract

Development of self-enhanced solid-state ECL platform creates a straightforward experimental design for the fabrication of point-of-care applications. Herein, we develop a promising method for self-enhanced solid-state ECL platform of polyluminol gold nanocomposite on glassy carbon electrode ((PL-Au)nano/GCE) via simple one step electrochemical deposition process without involving any additional co-reactants. The presence of AuNPs augments the electron transfer kinetics of PL and enhances the solid-state ECL intensity and promotes label free, excellent sensitivity, and selectivity to detect Hg2+ in physiological pH through signal-on mode. Unlike pristine PL/GCE, electrochemically co-deposited AuNPs in the (PL-Au)nano/GCE composite, enable the co-reactant accelerator by improving the catalytic activity of PL towards oxygen reduction reaction (ORR) yielding in-situ ROS (co-reactant) generation. Further, the ECL intensity of (PL-Au)nano/GCE composite, gradually increases by each addition of Hg2+ ion. This is because of the formation of an amalgamation of Au-Hg on (PL-Au)nano/GCE composite surface which further accelerate the yield of in-situ ROS and enhance the intensity of ECL. Whereas no ECL signals changes were observed for PL/GCE composite. The proposed self-enhanced solid-state ECL platform is selectively sensing the Hg2+ ion in the linear range of 0.3 nM to 200 nM with a detection limit of 0.1 nM. The demonstrated (PL-Au)nano/GCE platform might pave new avenues for further studies in the solid-state ECL platform which could be more useful in on-site monitoring of clinical bioassay and immunosensors.

Introduction

Electrogenerated-chemiluminesence (ECL) is a process of light emission which is due to an energetic interaction between electrogenerated species on electrode and electrolyte interface.[1] ECL has a great advantage over chemiluminescence (CL) because of low background signals, simple optical setup, good spatial-temporal control and versatility.[2,3] Recently, ECL becomes a popular and widely used analytical technique in clinical diagnostics, material science and environmental monitoring.[4,5] Even though $Ru(bpy)_3^{2+}$ based ECL-active luminophores systems have been reported in literature such as $Ru(bpy)_3^{2+}$-TprA,[6] $Ru(bpy)_3^{2+}$-$C_2O_4^{2-}$[7] and $Ru(bpy)_3^{2+}$-H_2O_2,[8,9] luminol-H_2O_2[10] based ECL systems has more attractive glance because of its non-toxicity, cost-efficient and high quantum yield with low oxidation potential.[11,12] The luminescent property of luminol-H_2O_2 system mostly depends on its inherent chemical or electrochemical reaction through the intermediates of oxygen species like $OH^{\bullet}$, $OH^{-\bullet}$ and $O_2^{-\bullet}$.[13,14] The major limitation of luminol's ECL property is hampered by its poor aqueous solubility, alkaline mediated ECL dependency. To overcome this, water soluble luminol derivatives were chemically synthesized with enhanced ECL intensity in aqueous electrolyte.[15] However, the adopted synthesis involves multiple steps, desires tedious reactions without scalability. Moreover, the co-reactant like H_2O_2 is also not quite stable at room temperature which also suppresses the efficiency of ECL signal of luminal.[16] One can overcome this problem by generating the reactive oxygen species (ROS) by using co-reactant accelerators which can produces more ROS through the reduction of dissolved oxygen and enhances the stability of ECL

signal.[17] In ECL, the co-reaction or co-reactant accelerators are playing a crucial role in boosting the ECL intensity of luminophore by dissociating the co-reactant into active radicals.[18] For example, the ECL intensity of Luminol in O_2 saturated electrolyte increased by 2-fold by the co-reactant accelerator strategy.[19]

Because of mass transport limitation, homogeneous phase or solution based luminol system always inhibits the efficiency of ECL emission, impeding the low molecular detection of selected analytes.[20–22] Use of heterogeneous or solid-state ECL has several advantages such as a minimum amount of luminophores is sufficient, simplifies the experimental setup, enhance more ECL intensity.[23–25] In this context, luminol is an aniline monomer derivative having an ECL inert $–NH_2$ group facilitating the electro-polymerization in acidic solution to form a stable polyluminol (PL) film on the electrode surface.[26] However, the PL films have less electrical conductivity in neutral or alkaline solution, which need further improvisation for highly efficient luminol system. Despite of few attempts taken in functionalizing the luminol system in solution state with metal NPs, till now no efforts were taken to hybridize PL films particularly at solid-state, which eventually have potential scope for point-of-care/on-site application.

Mercury ion (Hg^{2+}) is a heavy metal known for individual as well as environmental toxicity.[27] The presence of Hg^{2+} in human body causes brain damage and other chronic diseases.[28,29] Enzymes like horseradish peroxidase,[30] glucose oxidase,[31] invertase[32] and urease[33] has strong affinity with Hg^{2+} which inhibits the enzymes functions of human body. Therefore, the sensitive and selective method requires in detecting Hg^{2+} at a lower level is highly beneficial for environmental application as well as healthcare. Though spectroscopic and chromatorgraphic techniques are well documented as well as in practice for detection of Hg^{2+}, nevertheless modern analytical methods demand highly sensitive yet selective portable assay platform. Even though luminol based ECL property is established for Hg^{2+} estimation, still it requires specific bio-receptors like DNA[34] and enzymes[35] for selective ECL quenching. Thus, there is a potential need for the development of label-free solid-state ECL platform beneficial for selective detection of Hg^{2+} ion.

Herein, a simple one step electrochemical strategy is established for the preparation of $(PL\text{-}Au)_{nano}$/GCE which displayed the self-enhanced solid-state ECL signal, thereby enabling label-free detection of Hg^{2+} *via* signal-on ECL mode. Incorporation of electrochemically co-deposited AuNPs with PL films acts as co-reactant accelerator to enhancing the ECL intensity by producing more ROS. The optimized condition is selective for Hg^{2+} detection without influence from other metal ions. The obtained results were superior/specific to Hg^{2+} ion over the pristine PL/GCE and other noble metal composites $(PL\text{-}Pt)_{nano}$/GCE and $PL\text{-}Ag)_{nano}$/GCE. Hence, the *in-situ* generated ROS is utilized as co-reactant, the proposed methodology not requires any addition of co-reactant in to electrolyte to study the ECL of PL.

Experimental Section

2.1 Chemicals

Luminol (97%), Disodium hydrogen phosphate ($Na_2HPO_4.7H_2O$), Sodium dihydrogen phosphate mono hydrate ($NaH_2PO_4.H_2O$), Tetrachloroauric (III) acid (99.9%), hexachloroplatinic acid (IV) acid (99.9%), Sulphuric acid (18.3 M), Mercury chloride ($HgCl_2$), Silver nitrate (99.99%) and all other metal salts were purchased from Sigma Aldrich. All the chemicals were used without any further purification. Argon and Oxygen gas of 99.99% used to saturate the electrolyte solutions. Milli-Q water (18.2Ω) used as a solvent for preparing the electrolyte solution. 0.5 M H_2SO_4 stock solution was prepared by diluting 18.3 M H_2SO_4.

2.2 Electrochemistry and ECL measurements

Commercially available glassy carbon electrode (GCE) with 0.0732 cm^2 surface area serves as working electrode, platinum foil as the counter electrode and Ag/AgCl is used as reference electrode respectively. Cyclic voltammetry (CV) and potential step experiments were performed with an Autolab electrochemical workstation (EcoChemie, The Netherlands). The ECL along with CV signals is measured simultaneously with a photomultiplier tube (PMT, Hamamatsu H9305-04). The PMT was held at −500 V with a high-voltage power supply. The photo current generated at the PMT was converted to a voltage using an electrometer system (model 6517, Keithley, Cleveland,OH) and connected to the Autolab via an analog-to-digital converter (ADC).

2.3 Preparation of PL/GCE and $(PL\text{-}Au)_{nano}$/GCE

PL-Au nano-composite was electrochemically deposited on GCE as follows. Initially GCE was successively polished with Al_2O_3 slurry (0.3, 0.05 μm) then sonicated for 5 minutes in an ultrasonic bath with distilled water at room temperature. Further GCE was electrochemically cleaned in 0.5 M H_2SO_4 by cycling at 0.1 V/s from 0 to 1.2 V *vs.* Ag/ AgCl for 10 cycles. After that, polished GCE was immersed in electrochemical cell containing 1 mM luminol in 0.5 M H_2SO_4 and electrochemically treated about 20 cycles in the range of 0 to 1 V at the scan rate of 0.1 V/s (Fig. 1A). After the electrochemical treatment, the electrode was washed thoroughly with milliQ water, the modified electrode was termed as PL/GCE. Similar way $(PL\text{-}Au)_{nano}$/GCE prepared by taking 1 mM luminol +1.5 mM $HAuCl_4$ in 0.5 M H_2SO_4 (Fig. 1B). The electrode modification process also represented in scheme 1A.The same procedure was followed to deposit $(PL\text{-}Pt)_{nano}$ and $(PL\text{-}Ag)_{nano}$ on GCE using 1 mM luminol+1.5 mM $PtCl_4^{2-}$ and 1 mM luminol+1.5 mM $AgNO_3$ respectively, in 0.5 M H_2SO_4 which can be referred as $(PL\text{-}Pt)_{nano}$/GCE and $(PL\text{-}Ag)_{nano}$/GCE.

2.4 Characterization techniques

We used Field emission scanning electron microscope (FESEM, Supra 55 VP, Carl Zeiss), Energy dispersive X-ray (EDX, Oxford Instruments X-MAX, 20 mm²) analysis and Atomic force microscope (AFM, Agilent technologies 5500 instrument) technique in order to know the morphological changes and elemental presence after modification of GCE. The X-ray photoelectron spectroscopic (XPS) technique used to predict the state of elements present in the outermost part of composite by using Theta Probe AR-XPS System, Thermo Fisher Scientific (U.K).

2.5 ECL spectrum

ECL spectrum is recorded using the optimized PMT voltage as 950 V and slit width is 20 nm in spectrofluorimeter. Also, applied a constant potential pulse at 0.6 V vs Ag/AgCl on $(PL\text{-}Au)_{nano}$/glassy carbon plate (1x1 cm^2) in oxygen saturated 0.1 M PBS at pH 7.4.

Results And Discussions

3.1 Electrochemical studies of PL/GCE and $(PL\text{-}Au)_{nano}$/GCE

Fig. 1A &B depicts the cyclic voltammetry of PL and $(PL\text{-}Au)_{nano}$ growth pattern on glassy carbon substrate. As seen in Fig. 1A, a sharp increase in peak current at 0.9 V for the 1^{st} cycle of CV which is due to the luminol oxidation where the radical polymerization of luminol starts and decreased in the peak current (at 0.9 V) during the subsequent electrochemical cycling. Moreover, there is a reversible redox peak growth which is due to the reduction (E_{Pc}= 0.6 V) and oxidation (E_{pa}= 0.7 V) of PL. The redox peaks current are gradually increases for initial few cycles (up to 10 cycles) and then exhibit stable redox response without further increase in redox peak current. Interestingly, the existence of $HAuCl_4$ with luminol causes incremental redox peak current density of PL during electrochemical cycling without change in inherent redox potential. In addition, a small reduction peak at 0.8 V observed which is due to the reduction of Au^{3+} to Au^0 (Fig. 1B). To ensure this particular reduction reaction a control experiment with pristine $HAuCl_4$ was performed. To this only $HAuCl_4$ is dissolved in 0.5 M H_2SO_4 without luminol yield at sharp reduction peak at exactly 0.8 V and decreased upon continuous electrochemical cycling (Fig. S1A). After electrochemical cycling, the typical redox response of modified GCE (AuNPs/GCE) in 0.5 M H_2SO_4 confirms the formation of AuNPs on GCE (Fig. S1B). The CV of typical stable redox response of PL/GCE and $(PL\text{-}Au)_{nano}$/GCE clearly seen in the potential window of 0 to 1 V in 0.5 M H_2SO_4 solution (Fig. S2A,B), evidencing the deposition of PL.[36] However, the sweeping potential region is extended up to 1.7 V (Fig. S3) to validate the existence of typical redox characteristics of AuNPs in line with redox peaks of PL (at 0.7 V and 0.6 V). From the second cycle onwards the redox peak of PL is started to disappear with retention of AuNPs characteristic redox behavior, suggesting an over oxidation potential resulted from either leaching or deactivating the PL in 0.5 M H_2SO_4. And also, the calculated AuNPs reduction peak

charge in AuNPs/GCE (Fig. S1B) is almost 2-fold less when compared with the reduction charge of AuNPs in the $(PL\text{-}Au)_{nano}$/GCE (Fig. S3). Moreover, the peak current and charge associated with oxidation (at 0.7 V) and reduction (at 0.6 V) peak of PL in $(PL\text{-}Au)_{nano}$/GCE is also higher than that of pristine PL/GCE (Table S1). This is because of simultaneous growth deposition of AuNPs and PL film on GCE.

The surface morphology of electrochemically deposited PL/GCE and $(PL\text{-}Au)_{nano}$/GCE were studied by using FE-SEM (Fig. 1C-D). PL/GCE shows microstructures of polymer islands (Fig. 1C), on the other hand $(PL\text{-}Au)_{nano}$/GCE exhibit a homogenous spherical nanostructures with an average size distribution of ~60 nm (Fig. 1D), evidencing the existence of nanocomposite on GCE. To elucidate the elemental compositions and surface chemistry of the nanocomposite on GCE surface an XPS study was performed. Survey spectra of the prepared platform were presented in Fig. S4. The high resolution XPS spectra of Au $4f_{7/2}$ and Au $4f_{5/2}$ is denoted in Fig. 1E. The observed binding energies are in comparable with the standard values of pure gold *viz.,* 83.8 eV (CAS No.7440-57-5) and 87.43 eV (CAS No.7440-57-5) corresponded to $4f_{7/2}$ and $4f_{5/2}$, respectively. In order to understand the localization pattern of Au and PL films an *in-situ* etching was performed using with XPS analysis. Fig. 1F illustrates the XPS spectrum of etched $(PL\text{-}Au)_{nano}$/GCE with an amplified signal intensity of Au $4f_{7/2}$ and $4f_{5/2,}$ revealing enhanced exposure of Au *via* stripping of PL. This was further supported by the existence of weaker O1s and N1s peaks (Fig. S5). To complement the surface topography and elemental structure an AFM and EDX spectral measurements were performed and the results are presented in Fig. S6. The EDX of PL/GCE is shows C, N and O elements (Fig. S6A) whereas Au along with C and O presents in $(PL\text{-}Au)_{nano}$/GCE composite (Fig. S6B), which evidencing the PL and Au co-deposition on GCE surface. In addition, the AFM analysis is also displays macrostructure kind of morphology for PL/GCE (Fig. S6C), but nanostructured with spherical shapes presents in $(PL\text{-}Au)_{nano}$/GCE composite (Fig. S6D) as similar with FE-SEM. Electrical conductivity and charge transfer kinetics for the prepared $(PL\text{-}Au)_{nano}$/GCE was measured using electrochemical impedance spectroscopy (EIS). The calculated charge transfer resistance (ΔR_{ct}) derived from the Nyquist plot of PL/GCE and $(PL\text{-}Au)_{nano}$/GCE is 4076 Ω and 276 Ω, respectively (Fig. S7). The lesser value of R_{ct} clearly confirms that the $(PL\text{-}Au)_{nano}$/GCE exhibit better electrical conductivity and charge transfer kinetic than the pristine PL/GCE.

3.2 ECL experiments

Unlike redox response of $(PL\text{-}Au)_{nano}$/GCE in 0.1 M H_2SO_4 (Fig. S2A&B), the simultaneously recorded CV showed an irreversible peak at -0.4 V and 0.6 V which is due to the dissolved oxygen reduction reaction (ORR)[37] and PL oxidation peak (Fig. 2A.a) in O_2 gas saturated 0.1 M PBS (pH 7.4) during scanning from 0 to -0.8 V to +1 V. In contrast, the pristine PL/GCE showed oxidation peak at 0.6 V but the oxygen reduction peak observed at high cathode potential of -0.65 V (Fig. 2A.b). The less cathode peak potential shift approximately -0.25 V and high reduction current density for dissolved O_2 reduction clearly indicates that the $(PL\text{-}Au)_{nano}$/GCE is highly catalytic than pristine PL/GCE. To understand the role of AuNPs, the

PL film also deposited on polycrystalline gold surface (PL/pc-Au) which exhibit the redox response in O_2 gas saturated 0.1 M PBS (pH 7.4) (Fig. 2A.c). Although the peak potentials of PL oxidation and ORR are similar to the $(PL\text{-}Au)_{nano}$/GCE, the peak current density of PL oxidation and ORR is quite decreased. This further confirms the $(PL\text{-}Au)_{nano}$/GCE shows superior electro-catalytic behavior towards ORR. The simultaneous record of ECL from these modified electrodes shown in Fig. 2B. As expected, high intense ECL peak was observed at 0.6 V where exactly an oxidation of PL peak exist (Fig. 2A.a) in $(PL\text{-}Au)_{nano}$/GCE. The relative intensity of observed ECL signal of $(PL\text{-}Au)_{nano}$/GCE is almost three times higher than PL/GCE (Fig. 2B.b) and PL/pc-Au (Fig. 2B.c) composites. Under completely argon gas saturated 0.1 M PBS, the $(PL\text{-}Au)_{nano}$/GCE shows the disappearance of ORR and ECL peak (Fig. 2A.d&2B.d). All these results clearly confirm that, obtained ECL signals are totally dependent on the concentration of dissolved O_2 present in the electrolyte solution. The *in-situ* generated reactive oxygen species (ROS) from dissolved O_2 act as co-reactant which eventually react with PL anion to produce ECL signal. The ECL enhancement of $(PL\text{-}Au)_{nano}$/GCE is perhaps due to the presence of AuNPs which behaves as co-reactant accelerator by producing the ROS radicals *via* ORR. In order to understand the significance of AuNPs on PL film, the same PL film electrodeposited in the presence of H_2PtCl_4 and $AgNO_3$ with in the same experimental conditions of $(PL\text{-}Au)_{nano}$/GCE (Fig. S8A,B). Interestingly, there is no ECL observed for $(PL\text{-}pt)_{nano}$/GCE and $(PL\text{-}Ag)_{nano}$/GCE composites (Fig. S8C,D). Owing to its well-known catalytic behavior of Pt in ORR, the reduction of O_2 to H_2O occurs *via* direct $4e^-$ pathway and it may not follow $2e^-$ pathway which is necessary for H_2O_2 and ROS generation.[38,39] Even though luminol and Ag has good interaction and enable excellent chemiluminescence activity in presence of H_2O_2.[40]The present experimental conditions doesn't show any ECL for $(PL\text{-}Ag)_{nano}$/GCE suggesting $(PL\text{-}Ag)_{nano}$/GCE film could not act as ROS generator in solid-state ECL platform. Thus, the only AuNPs present in $(PL\text{-}Au)_{nano}$/GCE has effective co-competence of co-reactant accelerator to generate more ROS thereby promoting the ECL activity. Further, the effect of potential window on ECL intensity was studied by varying the initial potentials. Fig. 3A&B shows the CV and corresponding ECL responses of $(PL\text{-}Au)_{nano}$/GCE composite at various scan directions such as, 0 to 1 V, -0.3 to 1 V, -0.6 to 1 V and -0.8 to 1 V respectively in O_2 saturated 0.1 M PBS (pH 7.4). As illustrated in Fig. 3B, ECL intensities of $(PL\text{-}Au)_{nano}$/GCE composite vary on change of potential scan direction. We observed high intense ECL signal for -0.8 to 1 V (Fig. 3B.d) scans direction, because at this particular direction maximum amount of ROS generated by reduction of O_2 (Fig. 3A.d). A small intense ECL signal is observed when we scan 0 to 1 V. Overall, the ECL intensity of $(PL\text{-}Au)_{nano}$/GCE composite gradually increases by changing the potential scan towards more negative to positive direction and concluded that, ECL of $(PL\text{-}Au)_{nano}$/GCE composite is depends on the *in-situ* generated ROS. The ROS further oxidizes during anodic direction then reacts with poly luminol anion to emit light.

3.3 ECL stability

Since ECL signal of $(PL\text{-}Au)_{nano}$/GCE composite is depends on the *in-situ* generated ROS, we performed a time based ECL transient experiments by changing the initial stepping potentials to study the ECL stability of ROS in O_2 saturated 0.1 M PBS (pH 7.4). Fig. 4A shows the ECL intensity *vs.* time transients of $(PL\text{-}Au)_{nano}$/GCE composite at various initial potentials such as 0 (about 6 s) to 0.6 V (2.5 s), -0.3 (6 s) to 0.6 V (2.5 s), -0.6 (6 s) to 0.6 V (2.5 s) and -0.8 (6 s) to 0.6 V (2.5 s) respectively in O_2 saturated 0.1 M PBS (pH 7.4). The obtained ECL signals are quite stable even up to 18 consecutive cycles at various initial step potentials. Among different initial potential pulse, the potential pulse between -0.8 to 0.6 V, displays more intense and stable ECL signals which may be ascribed to the generation of more number of ROS at the interface of $(PL\text{-}Au)_{nano}$/GCE (Fig. 4A).

The ECL spectrum of $(PL\text{-}Au)_{nano}$/GCE (Fig. 4B) also performed to elucidate the wavelength of PL at various initial potentials in O_2 saturated 0.1 M PBS (pH 7.4). As seen from Fig. 4B, ECL signals were observed only at 430 nm which is consistent with photoluminescence spectrum. Further, the highest intensity of ECL spectrum is obtained for the pulse potential of -0.8 to 0.6 V, indicating the highest ROS generation in the specified potentials. This again complements the consistent of ECL transient experiment results (*vide supra*).

3.4 ECL study at various compositions

To validate the ECL experimental conditions and its associated effect of ECL intensity of $(PL\text{-}Au)_{nano}$/GCE, the different concentrations of luminol and $HAuCl_4.3H_2O$ were taken for electro-deposition (see in supporting information, section 2). From the experimental observation it is found that 1.5 mM of $HAuCl_4.3H_2O$ and 1 mM luminol is sufficient for deposition of $(PL\text{-}Au)_{nano}$/GCE composite, which apparently enabled a high intense ECL signal (Fig. S9, S10).

3.5 Effect of Hg^{2+} ion

It has been identified in the literature that, the AuNPs and Hg^{2+} ion has strong specific metallophilic interaction and form spontaneous Au-Hg amalgam which tunes the catalytic properties of AuNPs and accelerate the rate of decomposition of H_2O_2.[41]Such study can be escalated for various applications particularly in environmental pollutant monitoring, and detection of Hg^{2+} as preservatives in vaccines. Inspired from that herein, the effect of Hg^{2+} ion with $(PL\text{-}Au)_{nano}$/GCE by exploring the various Hg^{2+} ion concentrations from 10 to 150 nM in O_2 saturated 0.1 M PBS (pH 7.4) at 0.1 V/s (Fig. S11A). Interestingly, the ECL intensity of $(PL\text{-}Au)_{nano}$/GCE linearly increases with each addition of Hg^{2+} ion and reaches maximum limit up to 150 nM, after that there is no much enhancement was observed. The observed enhancement of ECL intensity (signal on mechanism) during the addition of Hg^{2+} ion is due to the affinity between AuNPs and Hg^{2+} ion, leading to the formation of Au-Hg amalgam *via* aurophilic interactions.[41] As expected, the surface properties of AuNPs has been further changed upon interaction with Hg^{2+}, and

accelerate the *in-situ* generation of highly reactive ROS through catalytic reduction of dissolved oxygen.[42]The detailed ECL mechanism of $(PL\text{-}Au)_{nano}$/GCE before and after Hg^{2+} addition is shown in the scheme 1B. The calibration curve of ECL intensity versus Hg^{2+} ion concentrations were represented in Fig. S11B. A perfect linear relationship between ECL efficiency and Hg^{2+} concentrations were obtained from 10 to150 nM. Further we performed time *vs.* ECL intensity transient experiment to gain the better sensitivity. Fig. 5A depicts the obtained ECL transient curves at potentials pulse of holding the potential of – 0.8 V about 10 s and then 0.6 V held about 0.5 s in O_2 saturated 0.1 M PBS (pH 7.4). The ECL intensity of $(PL\text{-}Au)_{nano}$/GCE enhanced by the each addition of Hg^{2+} ion in the linear range of 0.3 to 200 nM (Fig. 5B). The detection limit or limit of detection (LOD) is obtained by using 3xstandard deviation/slope and the value is observed to be 0.1 nM and LOD is comparable with previous methods (Table 1). It is worthy to note that the similar experiments were also performed by using PL/GCE in the presence of Hg^{2+} ion at different concentrations and there is no change in ECL intensity of PL/GCE during the Hg^{2+} addition (Fig. S12). This results undoubtedly confirms that $(PL\text{-}Au)_{nano}$/GCE composite only capable of producing more ECL in the presence of Hg^{2+} ion.

Table 1

Comparison of Hg^{2+} linear range and limit of detection with previous reported methods.

Methods	Probes	Linear range	LOD	Ref
ECL	DNA labelled with ruthenium complex	1 nM to 1μM	0.3 nM	43
	BSA protected Au-Ag bi-metallic clusters			
ECL	Magnetic beads separation/collection process	10 nM to 5 μM	2.5 nM	44
ECL	$Ru(phe)_3^{2+}$/thymine on graphene oxide modified GCE	1 to 250 nM	5 nM	45
ECL	$Ru(bpy)_3^{2+}$doped silica nanoparticles		0.34 nM	46
	Au NPs-DNA probe			
ECL	MnO_2nanosheet	1 nM to 10 μM	2.3 nM	47
Fluorescence	$(PL\text{-}Au)_{nano}$/GCE		40 nM	
Fluorescence		5 nM to 50 μM	0.8 nM	48
ECL		80 nM to 6 μM	0.1 nM	49
		0 to 20 nM		In this work
		0.3 to 200 nM		

3.6 Interference study

In order to check the selectivity towards accelerator as well as detection of Hg^{2+} ion on $(PL\text{-}Au)_{nano}$/GCE using ECL method, other metal ions such as Fe^{2+}, Co^{2+}, Pb^{2+}, As^{2+}, Cu^{2+}, Cd^{2+}, and Mg^{2+} were also added during the ECL measurements. The interference study has performed by using i-t transient experiment by holding the potential of -0.8 V for 10 s and 0.6 V about 0.5 s. Fig. 5C shows the bar diagram of ECL intensity with respect to 100 µM of all metal ions using $(PL\text{-}Au)_{nano}$/GCE composite in O_2 saturated 0.1 M PBS (pH 7.4). It can be notified that the high intense ECL signal is only in the case of Hg^{2+} addition, on the other hand, ECL signal from $(PL\text{-}Au)_{nano}$/GCE against other studied metal ions were extremely low comparable to the bare system. The obtained results further evidencing the selectivity of the prepared $(PL\text{-}Au)_{nano}$/GCE system against the Hg^{2+}, suggesting an ideal platform for real sample analysis.

3.7 Real sample analysis

The Hg^{2+} ion in clinical samples like serum and environmental samples like tap water were tested by spiking the known concentrations. Initially, the tap water was boiled for few minutes to remove the contaminants, and then cooled at an open atmosphere until to reach the room temperature. Afterward, the known concentrations of Hg^{2+} were spiked into the water and performed the ECL experiments. To detect the Hg^{2+} ion in serum samples a known amount of Hg^{2+} spiked and recorded the ECL experiments. The recovery of sample were also calculated in both tap water and serum indicated in table 2. From the observed results we can say that the proposed strategy to detect Hg^{2+} in real sample analysis could be possible. The percentage recoveries of the analyte were in the range of 93 to 104 suitable for practical application (Table 2). Further, we compared the Hg^{2+} recovery in tap water and serum samples by using Atomic absorption spectroscope (AAS) technique. The standard Hg^{2+} ion solutions of 25, 50, 100, 150, 250, 300 and 500 nM were calibrated, the linear plot shown in Fig. S13 and the unknown concentrations of real samples were analyzed and shown in table S2. The obtained recovery (%) by AAS is consistent with adopted ECL method.

Table 2

Hg^{2+} ion detection in tap water and serum samples

Sample	Concentration		Recovery (% n=3)
	Spiked (nM)	found (nM)	
Tap water	30	28.3	94.3
	50	49.1	98.2
Serum	30	29.4	98.0
	50	52.2	104.4

Conclusions

In conclusion, we developed a co-reactant free solid-state ECL strategy by electro deposition of polyluminol-gold on GCE surface and observed a stable ECL signal in O_2 saturated neutral buffer solutions. The observed ECL intensity effectively increases with addition of Hg^{2+} ion even at picomolar range with good linear relationship. Even though the adopted methodology is simple and one pot synthesis procedure involved to prepare the self-enhanced solid state ECL platform. This is the first time we utilized luminol-gold probe to detect Hg^{2+} with signal-on ECL platform rather than quenching. Moreover, this co-reactant free novel solid-state self-enhanced ECL offers good recovery in the real sample analysis of Hg^{2+} ion sensing and obtained results were comparable with standard spectroscopic technique of atomic absorption spectroscope.

Declarations

CSIR-CECRI Manuscript Communication Number:

CECRI/PESVC/Pubs/2020-031

ACKNOWLEDGMENT

C.V. Raju thanks the CSIR for the award of Senior Research Fellowship (SRF) and S.S.K. thanks Department of Science and Technology (EMR/2017/004449) for their financial support.

References

1. White, H. S. & Bard, A. J. Electrogenerated Chemiluminescence and Chemiluminescence of the $Ru(bpy)_3^{2+}$-Peroxydisulfate System in Acetonitrile-Water Solutions. *J. Am. Chem. Soc* **104**, 6891–6895 (1982).
2. Venkateswara Raju, C. & Senthil Kumar, S. Highly sensitive novel cathodic electrochemiluminescence of tris(2,2'-bipyridine)ruthenium(II) using glutathione as a co-reactant. *Chem. Commun* **53**, 6593–6596 (2017).
3. Senthil Kumar, S. & Bard, A. J. Background Emission of Electrogenerated Chemiluminescence during Oxidation of Tri-n-propylamine from the Dimeric $^1\Delta g$ State of O_2. *Anal. Chem* **85**, 292–295 (2013).
4. Zhang, Z., Cui, H., Lai, C. & Liu, L. Gold Nanoparticle-Catalyzed Luminol Chemiluminescence and Its Analytical Applications. *Anal. Chem* **77**, 3324–3329 (2005).
5. Shen, J., Zhou, T. & Huang, R. Recent Advances in Electrochemiluminescence Sensors for Pathogenic Bacteria Detection. *Micromachines* **10**, 532 (2019).
6. Zu, Y. & Bard, A. J. Electrogenerated Chemiluminescence. 66. The Role of Direct Coreactant Oxidation in the Ruthenium Tris(2,2‘)bipyridyl/Tripropylamine System and the Effect of Halide Ions on the Emission Intensity. *Anal. Chem* **72**, 3223–3232 (2000).
7. White, H. S. & Bard, A. J. Electrogenerated chemiluminescence. 41. Electrogenerated chemiluminescence and chemiluminescence of the $Ru(2,2^1$-bpy$)32+$-$S_2O_8^{2-}$ system in acetonitrile-water solutions. *J. Am. Chem. Soc* **104**, 6891–6895 (1982).
8. Choi, J.-P. & Bard, A. J. Electrogenerated chemiluminescence (ECL) 79. *Anal. Chim. Acta* **541**, 141–148 (2005).
9. Irkham *et al.* Electrogenerated Chemiluminescence by in Situ Production of Coreactant Hydrogen Peroxide in Carbonate Aqueous Solution at a Boron-Doped Diamond Electrode. *J. Am. Chem. Soc* **142**, 1518–1525 (2020).
10. Mayer, M. *et al.* Shedding Light on the Diversity of Surfactant Interactions with Luminol Electrochemiluminescence for Bioanalysis. *Anal. Chem* **91**, 13080–13087 (2019).
11. Xu, S., Liu, Y., Wang, T. & Li, J. Highly Sensitive Electrogenerated Chemiluminescence Biosensor in Profiling Protein Kinase Activity and Inhibition Using Gold Nanoparticle as Signal Transduction Probes. *Anal. Chem* **82**, 9566–9572 (2010).
12. Gu, W. *et al.* Wenling Gu, Xi Deng, Xiaoxiao Gu, Xiaofang Jia, Baohua Lou, Xiaowei Zhang, Jing Li, and Erkang Wang. *Anal. Chem* **87**, 1876–1881 (2015).
13. Vitt, J. E., Johnson, D. C. & Engstrom, R. C. The Effect of Electrode Material on the Electrogenerated Chemiluminescence of Luminol Electrode Potential. *J. Electrochem. Soc* **138**, 1637–1643 (1991).
14. Zhang, Z. *et al.* Utilization and prospects of electrochemiluminescence for characterization, sensing, imaging and devices. *Mater. Chem. Front* **3**, 2246–2257 (2019).

15. Mayer, M. *et al.* Electrochemiluminescence Bioassays with a Water-Soluble Luminol Derivative Can Outperform Fluorescence Assays. *Angew. Chem. Int. Ed* **57**, 408–411 (2018).
16. Jiang, X. *et al.* A novel metal–organic framework loaded with abundant N-(aminobutyl)-N-(ethylisoluminol) as a high-efficiency electrochemiluminescence indicator for sensitive detection of mucin1 on cancer cells. *Chem. Commun* **53**, 9705–9708 (2017).
17. Gu, W. *et al.* Single-Atom Iron Boosts Electrochemiluminescence. *Angew. Chem. Int. Ed.*. **59**, 3534–3538 (2020).
18. Hu, L., Wu, Y., Xu, M., Gu, W. & Zhu, C. Recent advances in co-reaction accelerators for sensitive electrochemiluminescence analysis. *Chem. Commun* **56**, 10989–10999 (2020).
19. Yang, L. *et al.* Synthesis and Application of CeO_2 /SnS_2 Heterostructures as a Highly Efficient Coreaction Accelerator in the Luminol–Dissolved O_2 System for Ultrasensitive Biomarkers Immunoassay. *Anal. Chem* **91**, 14066–14073 (2019).
20. Gao, W., Xia, X. H., Xu, J. J. & Chen, H. Y. Three-dimensionally ordered macroporous gold structure as an efficient matrix for solid-state electrochemiluminescence of $Ru(bpy)_3^{2+}$/TPA system with high sensitivity. *J. Phys. Chem.C* **111**, 12213–12219 (2007).
21. Haghighi, B. & Bozorgzadeh, S. Enhanced electrochemiluminescence from luminol at multi-walled carbon nanotubes decorated with palladium nanoparticles : A novel route for the fabrication of an oxygen sensor and a glucose biosensor. *Anal. Chim. Acta* **697**, 90–97 (2011).
22. Maness, K. M., Terrill, R. H., Meyer, T. J., Murray, R. W. & Wightman, R. M. Solid-State Diode-like Chemiluminescence Based on Serial , Immobilized Concentration Gradients in Mixed-Valent. *J. Am. Chem. Soc* **118**, 10609–10616 (1996).
23. Collinson, M. M., Taussig, J. & Martin, S. A. Solid-State Electrogenerated Chemiluminescence from Gel-Entrapped Ruthenium (II) Tris (bipyridine) and Tripropylamine. *Chem. Mater* **11**, 2594–2599 (1999).
24. Xue, J. *et al.* Efficient Solid-State Electrochemiluminescence from High-Quality Perovskite Quantum Dot Films. *Anal. Chem* **89**, 8212–8216 (2017).
25. Maness, K. M. *et al.* olid State Electrochemically Generated Luminescence Based on Serial Frozen Concentration Gradients of Ru III / II and Ru II / I Couples in a Molten Ruthenium 2 , 2 ' -Bipyridine ComplexS. *J. Am. Chem. Soc* **119**, 3987–3993 (1997).
26. Li, G., Zheng, X. & Song, L. Electrochemiluminescence Characterization of Poly(luminol-benzidine) Composite Films and Their Analytical Application. *Electroanalysis* **21**, 845–852 (2009).
27. Bhattacharjee, Y. & Chakraborty, A. Label-Free Cysteamine-Capped Silver Nanoparticle-Based Colorimetric Assay for Hg(II) Detection in Water with Subnanomolar Exactitude. *ACS Sustainable Chem. Eng* **2**, 2149–2154 (2014).
28. Kraepiel, A. M. L. & Amyot, M. The chemical cycle and bioaccumulation. *Annu. Rev. Ecol. Syst* **29**, 543–566 (1998).

29. Onyido, I., Norris, A. R. & Buncel, E. Biomolecule–Mercury Interactions : Modalities of DNA Base–Mercury Binding Mechanisms. Remediation Strategies. *Chem. Rev* **104**, 5911–5929 (2004).
30. Han, S., Zhu, M., Yuan, Z. & Li, X. A methylene blue-mediated enzyme electrode for the determination of trace mercury (II), mercury (I), methylmercury , and mercury – glutathione complex. *Biosens. Bioelectron* **16**, 9–16 (2001).
31. Alexander, P. W. & Rechnitz, G. A. Enzyme Inhibition Assays with an Amperometric Glucose Biosensor Based on a Thiolate Self-Assembled Monolayer. *Electroanalysis* **5**, 343–350 (2000).
32. Soldatkin, O. O. *et al.* Novel conductometric biosensor based on three-enzyme system for selective determination of heavy metal ions. *Bioelectrochemistry* **83**, 25–30 (2012).
33. Pirvutoiu, S. *et al.* Flow injection analysis of mercury(II) based on enzyme inhibition and thermometric detection. *Analyst* **126**, 1612–1616 (2001).
34. Pavlov, V. *et al.* Amplified Chemiluminescence Surface Detection of DNA and Telomerase Activity Using Catalytic Nucleic Acid Labels. *Anal. Chem* **76**, 2152–2156 (2004).
35. Tao, X. *et al.* Development of a highly sensitive chemiluminescence enzyme immunoassay using enhanced luminol as substrate. *Luminescence* **29**, 301–306 (2014).
36. Ashok Kumar, S., Cheng, H.-W. & Chen, S.-M. Electroanalysis of ascorbic acid (vitamin C) using nano-ZnO/poly(luminol) hybrid film modified electrode. *React Funct Polym* **69**, 364–370 (2009).
37. El-Deab, M. S., Okajima, T. & Ohsaka, T. Electrochemical Reduction of Oxygen on Gold Nanoparticle-Electrodeposited Glassy Carbon Electrodes. *J. Electrochem. Soc* **150**, A851 (2003).
38. Sánchez-Sánchez, C. & Bard, A. Hydrogen peroxide production in the oxygen reduction reaction at different electrocatalysts as quantified by scanning electrochemical microscopy. *Anal. Chem* **81**, 8094–8100 (2009).
39. Jiang, Z., Jiang, Z., Tian, X. & Chen, W. Amine-functionalized holey graphene as a highly active metal-free catalyst for the oxygen reduction reaction. *J. Mater. Chem. A* **2**, 441–450 (2014).
40. He, Y., Liu, D., He, X. & Cui, H. One-pot synthesis of luminol functionalized silver nanoparticles with chemiluminescence activity for ultrasensitive DNA sensing. *Chem. Commun* **47**, 10692–10694 (2011).
41. Han, K. N., Choi, J. & Kwon, J. Gold nanozyme-based paper chip for colorimetric detection of mercury ions. *Sci Rep* **7**, 2806 (2017).
42. Zhang, S. *et al.* High-throughput and ultratrace naked-eye colorimetric detection of Au^{3+} based on the gold amalgam-stimulated peroxidase mimetic activity in aqueous solutions. Chem. Commun **53**, 5056–5058 (2017).
43. Yaping L. Electrogenerated Chemiluminescence Detection of Mercury (II) Ions Based on DNA Probe Labeled with Ruthenium Complex. *Anal Sci* **27**, 193–196 (2011).
44. Chao-Wei Tseng, Hsiang-Yu Chang, J.-Y. C. and C.-C. H. Detection of mercury ions based on mercury-induced switching of enzyme-like activity of platinum/gold nanoparticles. *Nanoscale* **4**, 6823–6830 (2012).

45. Li, Q., Zhou, X. & Xing, D. Rapid and highly sensitive detection of mercury ion (Hg) by magnetic beads-based electrochemiluminescence assay. *Biosens. Bioelectron* **26**, 859–862 (2010).
46. Gao, Y., Wang, T. & Liu, F. Determination of Hg^{2+} in Tap Water Based on the Electrochemiluminescence of $Ru(phen)_3^{2+}$ and Thymine at Bare and Graphene Oxide-Modified Glassy Carbon Electrodes. *Chinese Journal of Chemistry* **34**, 1297–1303 (2016).
47. Zhu, X., Chen, L., Lin, Z., Qiu, B. & Chen, G. A highly sensitive and selective 'signal-on' electrochemiluminescent biosensor for mercury. *Chem. Commun* **46**, 3149–51 (2010).
48. Wang, H., Wang, Y., Jin, J. & Yang, R. Gold nanoparticle-based colorimetric and 'turn-on' fluorescent probe for mercury(II) ions in aqueous solution. *Anal. Chem* **80**, 9021–9028 (2008).
49. Yang, K., Zeng, M., Hu, X. J., Guo, B. S. & Zhou, J. B. Layered MnO_2 nanosheet as a label-free nanoplatform for rapid detection of mercury(II). *Analyst* **139**, 4445–4448 (2014).

Figures

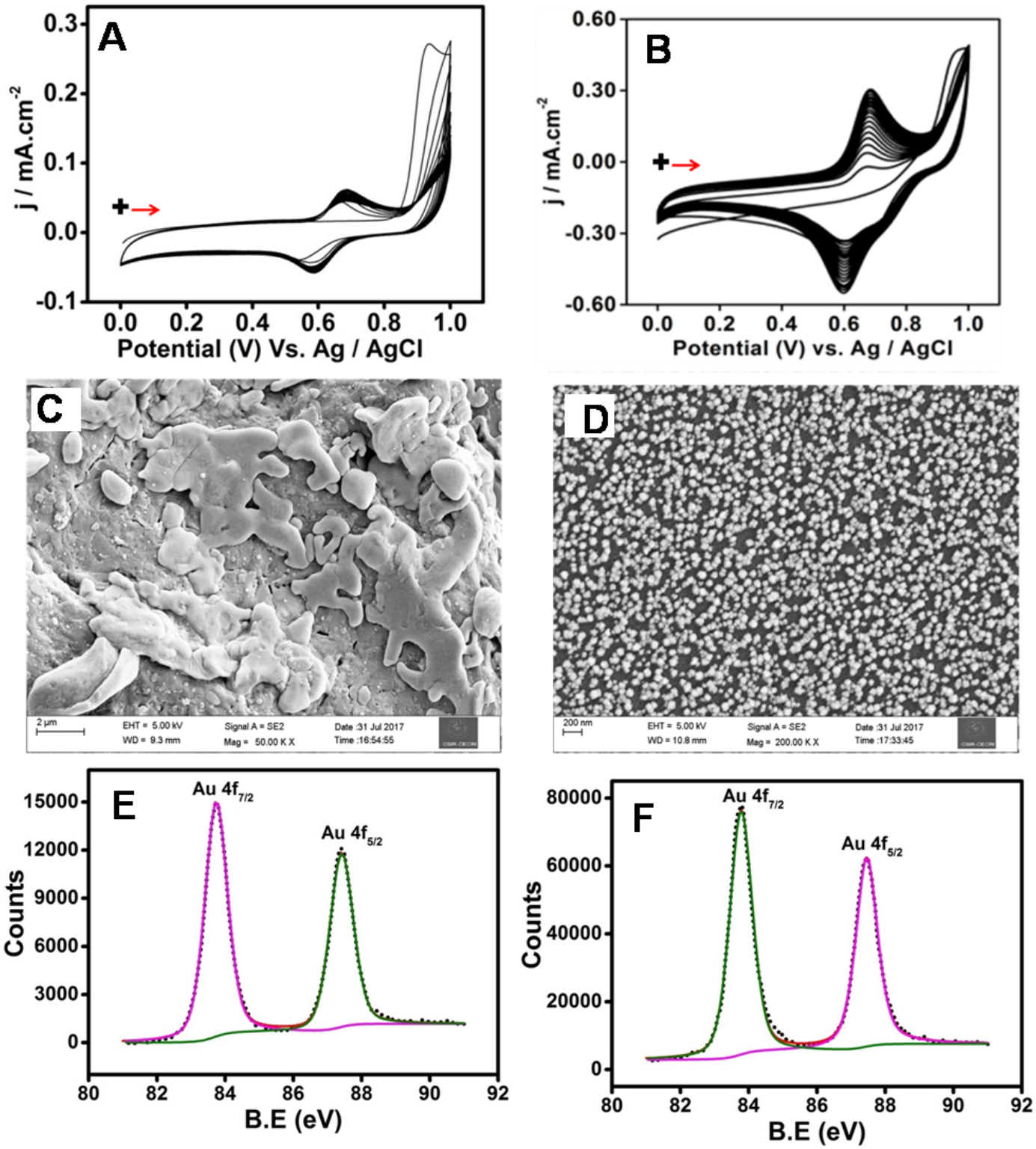

Figure 1

Repetitive CVs of 1 mM luminol (A) and 1 mM luminol+1.5 mM HAuCl4 (B) in 0.5 M H2SO4 at the scan rate of 0.1 V/s. FESEM images of PL/GCE (C) and (PL-Au)nano/GCE (D). The XPS spectrum (4f5/2 and 4f7/2 of Au) of (PL-Au)nano/GCE before and after etching (E,F) respectively.

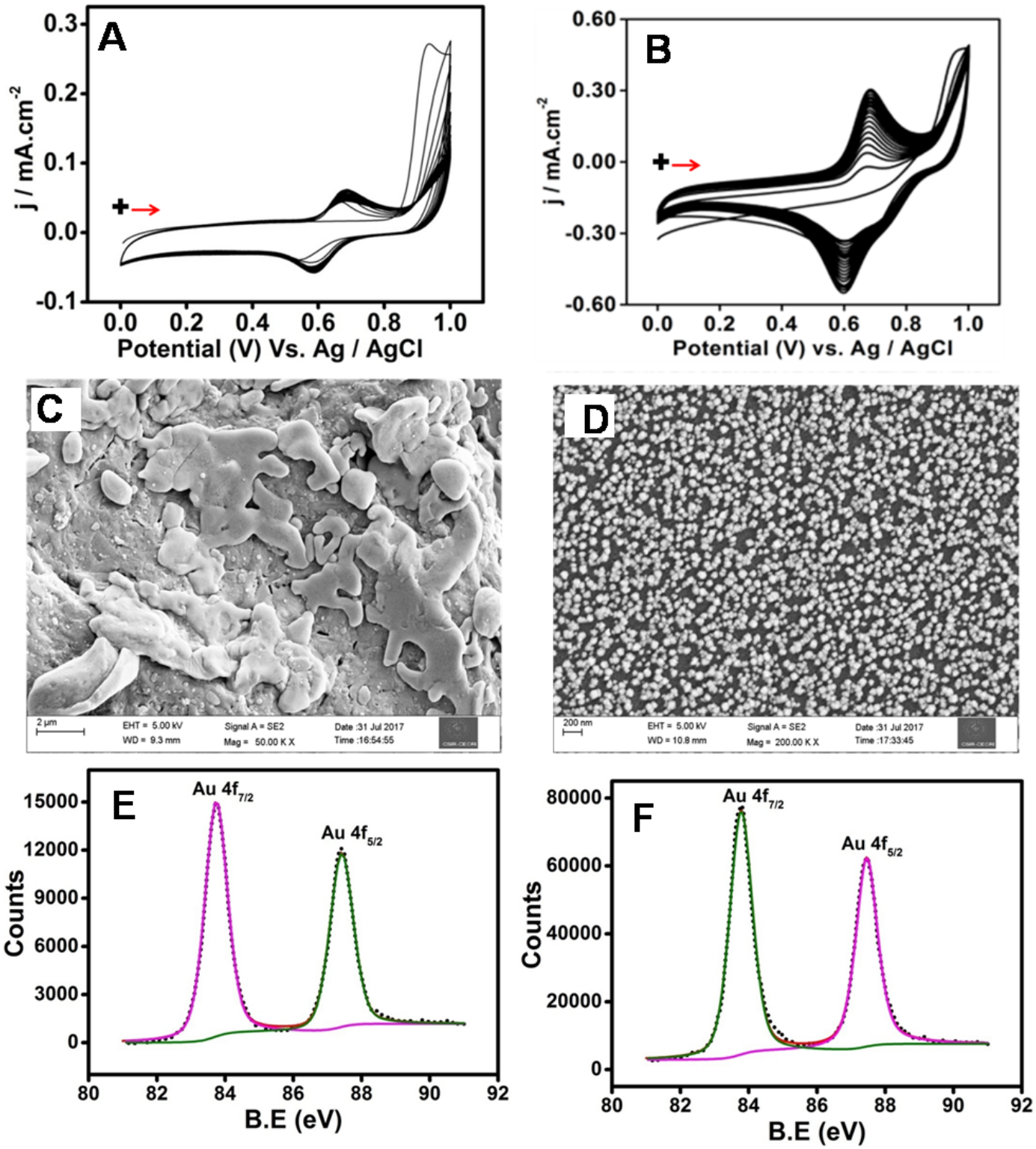

Figure 1

Repetitive CVs of 1 mM luminol (A) and 1 mM luminol+1.5 mM HAuCl4 (B) in 0.5 M H2SO4 at the scan rate of 0.1 V/s. FESEM images of PL/GCE (C) and (PL-Au)nano/GCE (D). The XPS spectrum (4f5/2 and 4f7/2 of Au) of (PL-Au)nano/GCE before and after etching (E,F) respectively.

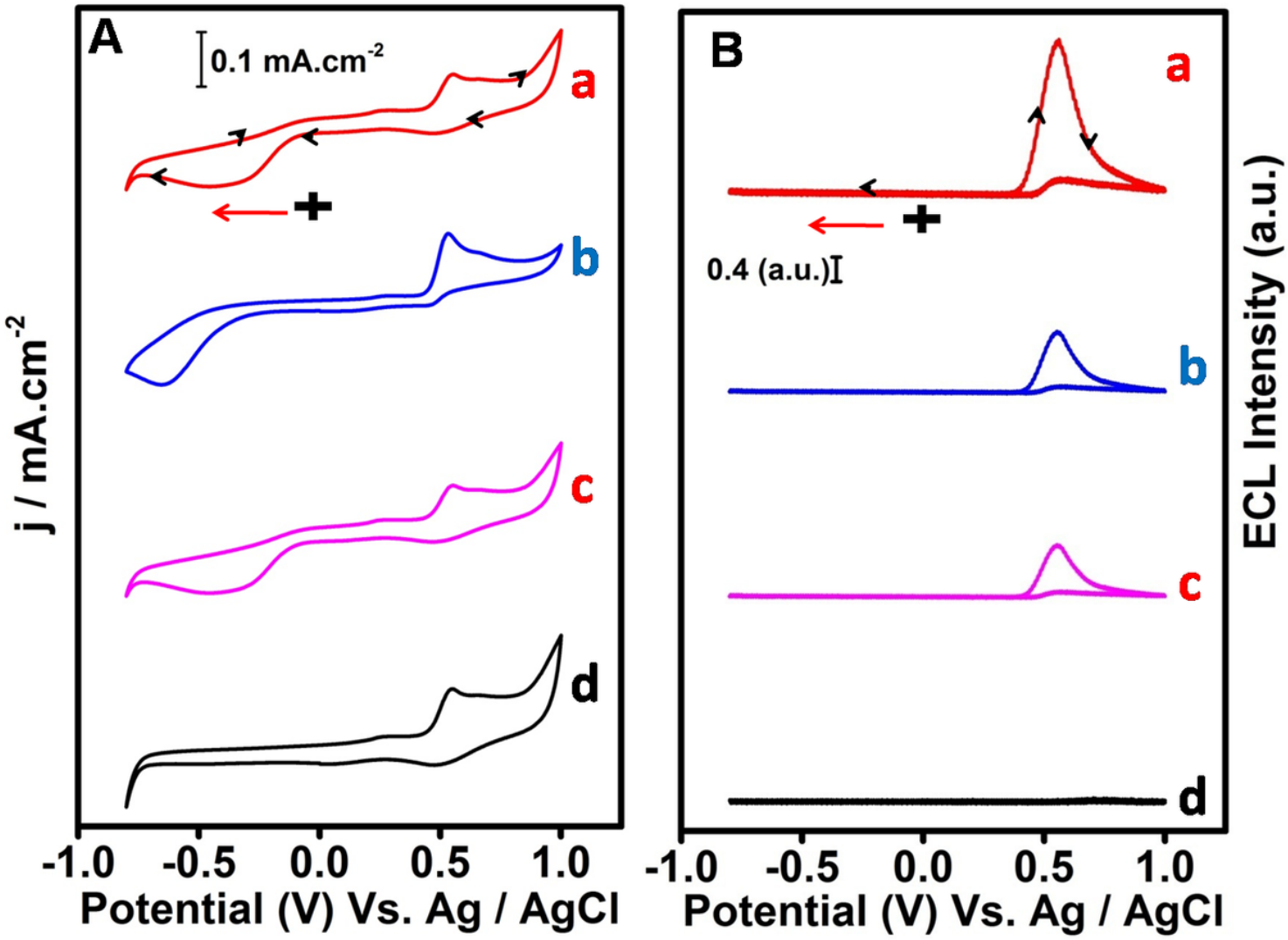

Figure 2

Simultaneously obtained CV (A) and its corresponding ECL responses (B) of (PL-Au)nano/GCE (a), PL/GCE (b), PL/pc-Au (c), in O2 saturated and (PL-Au)nano/GCE (d) in Argon saturated 0.1 M PBS (pH 7.4) at 0.1 V/s.

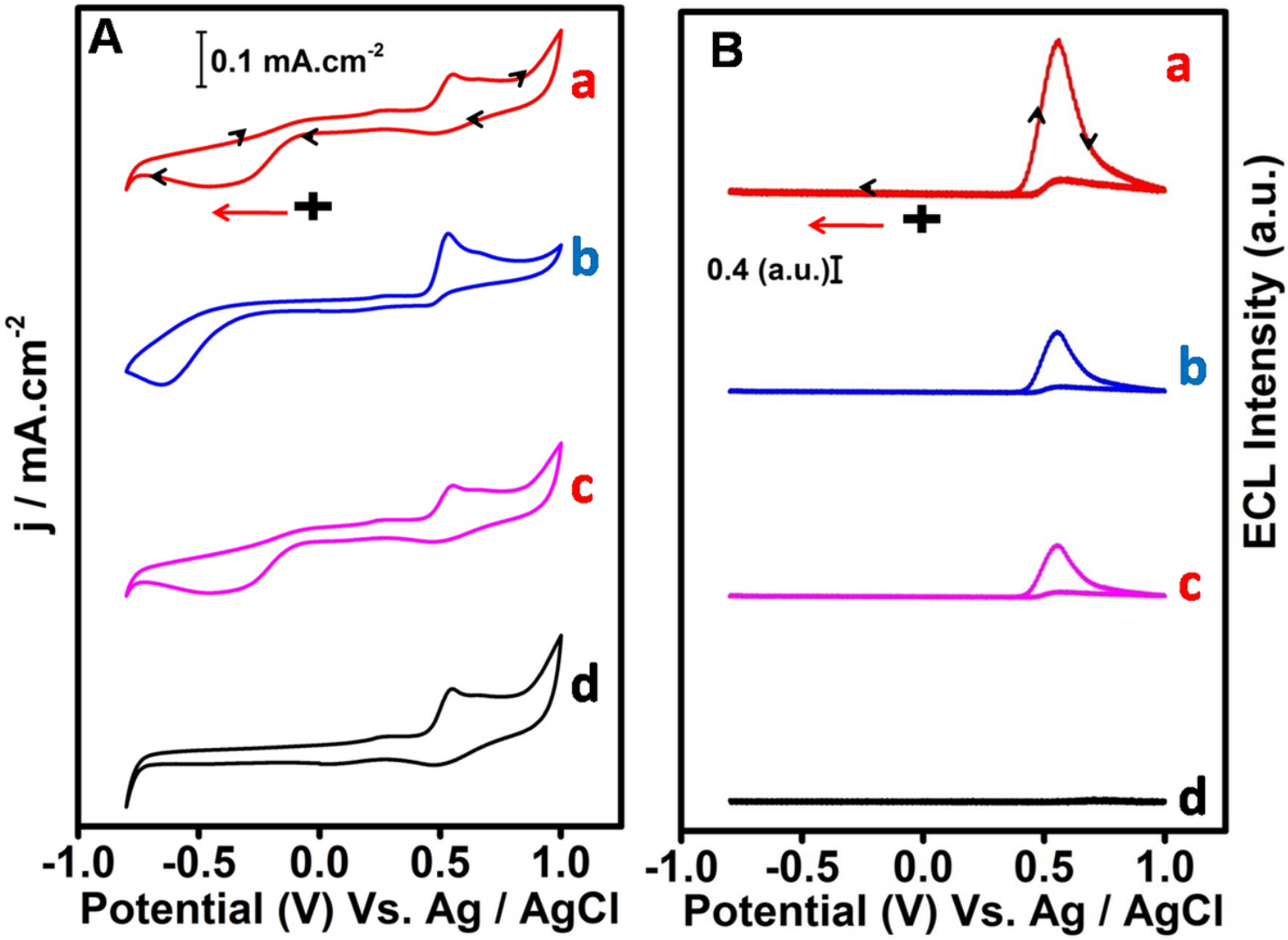

Figure 2

Simultaneously obtained CV (A) and its corresponding ECL responses (B) of (PL-Au)nano/GCE (a), PL/GCE (b), PL/pc-Au (c), in O2 saturated and (PL-Au)nano/GCE (d) in Argon saturated 0.1 M PBS (pH 7.4) at 0.1 V/s.

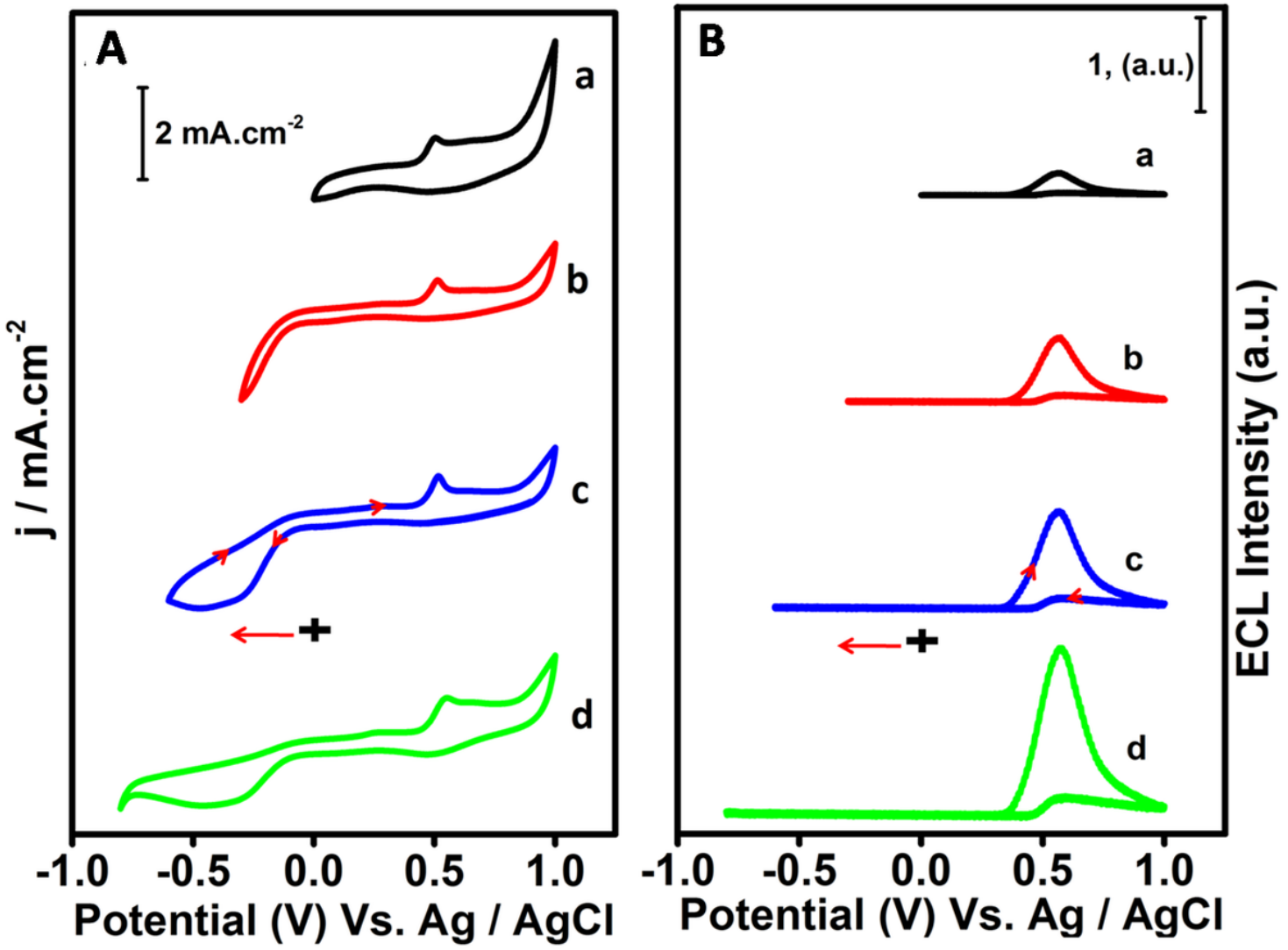

Figure 3

Cyclic voltammograms (A) and corresponding ECL signals (B) of (PL-Au)nano/GCE in O2 saturated 0.1 M PBS (pH 7.4) at several potentials, (a) 0 to 1 V, (b) -0.3 to 1 V, (c) -0.6 to 1 V and (d) 0 -0.8 to 1 V.

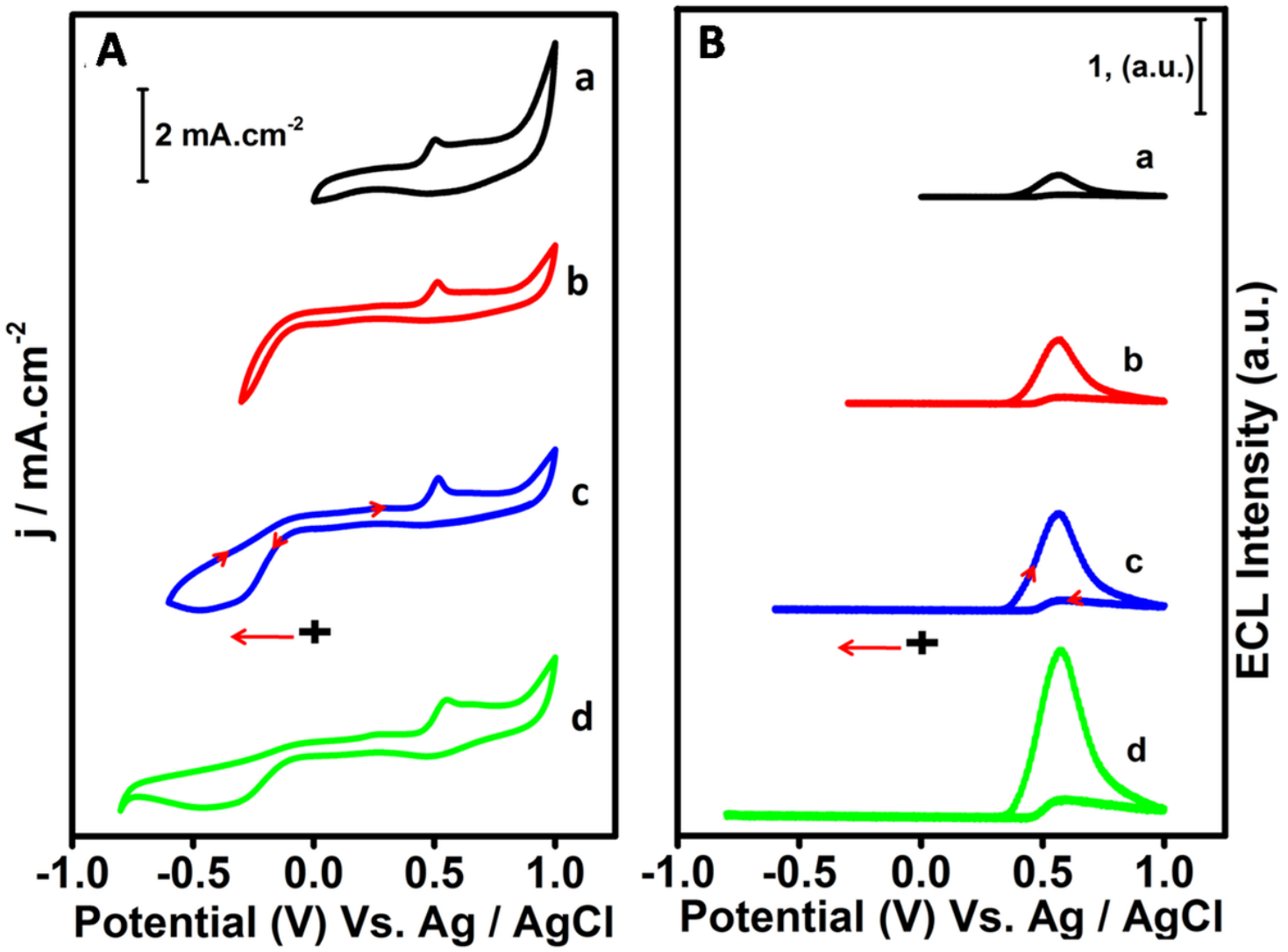

Figure 3

Cyclic voltammograms (A) and corresponding ECL signals (B) of (PL-Au)nano/GCE in O2 saturated 0.1 M PBS (pH 7.4) at several potentials, (a) 0 to 1 V, (b) -0.3 to 1 V, (c) -0.6 to 1 V and (d) 0 -0.8 to 1 V.

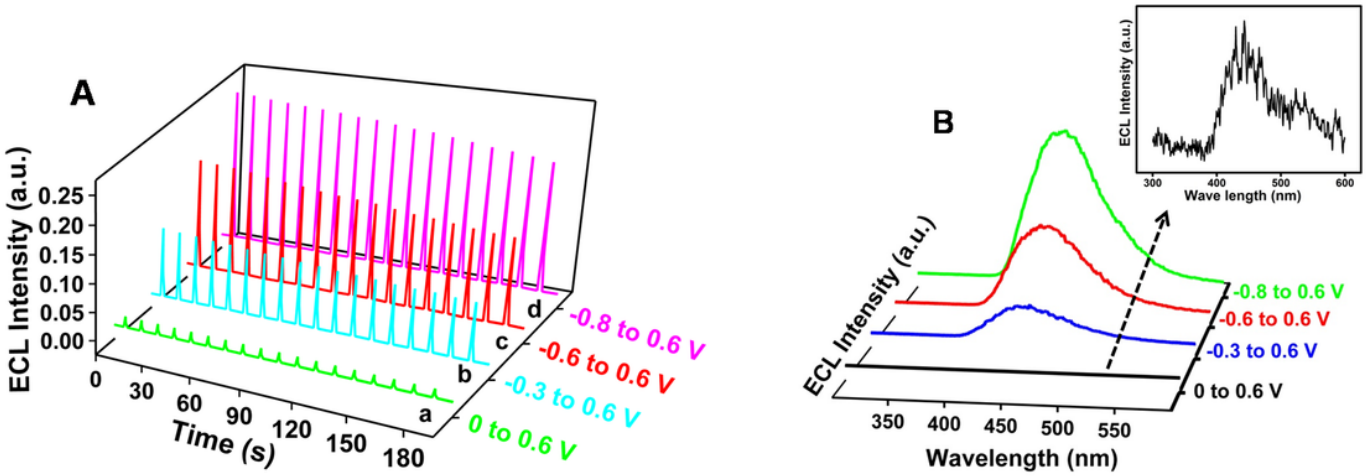

Figure 4

ECL intensity vs. time curves of (PL-Au)nano/GCE (A) and ECL spectrum (B) in O2 saturated 0.1 M PBS (pH 7.4) at several pulse potentials such as 0 to 0.6 V (a), -0.3 to 0.6 V (b), -0.6 to 0.6 V (c) and -0.8 to 0.6 V (d).

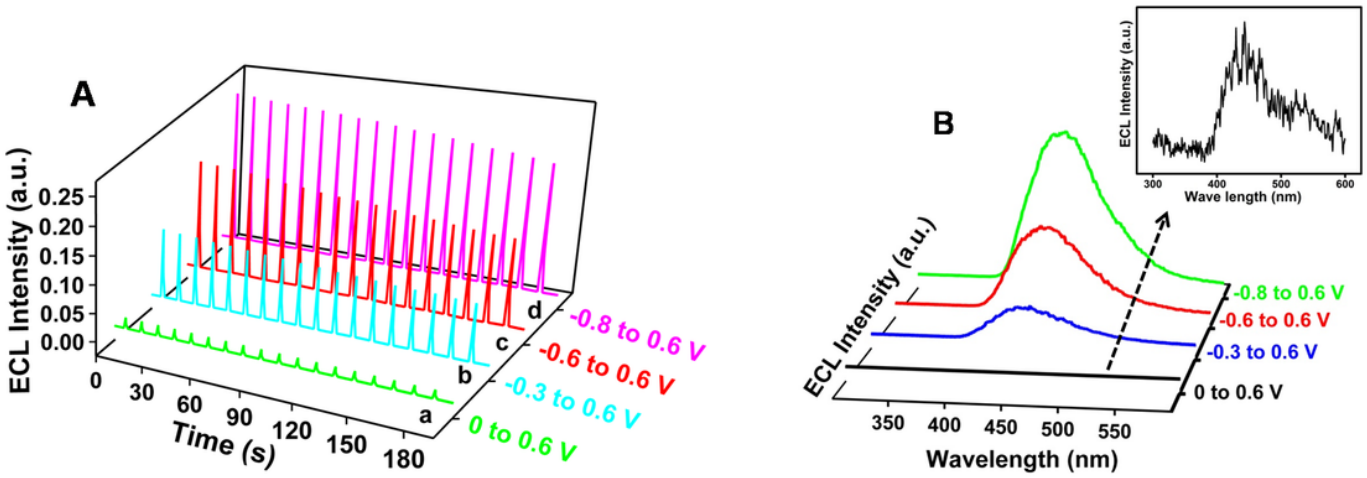

Figure 4

ECL intensity vs. time curves of (PL-Au)nano/GCE (A) and ECL spectrum (B) in O2 saturated 0.1 M PBS (pH 7.4) at several pulse potentials such as 0 to 0.6 V (a), -0.3 to 0.6 V (b), -0.6 to 0.6 V (c) and -0.8 to 0.6 V (d).

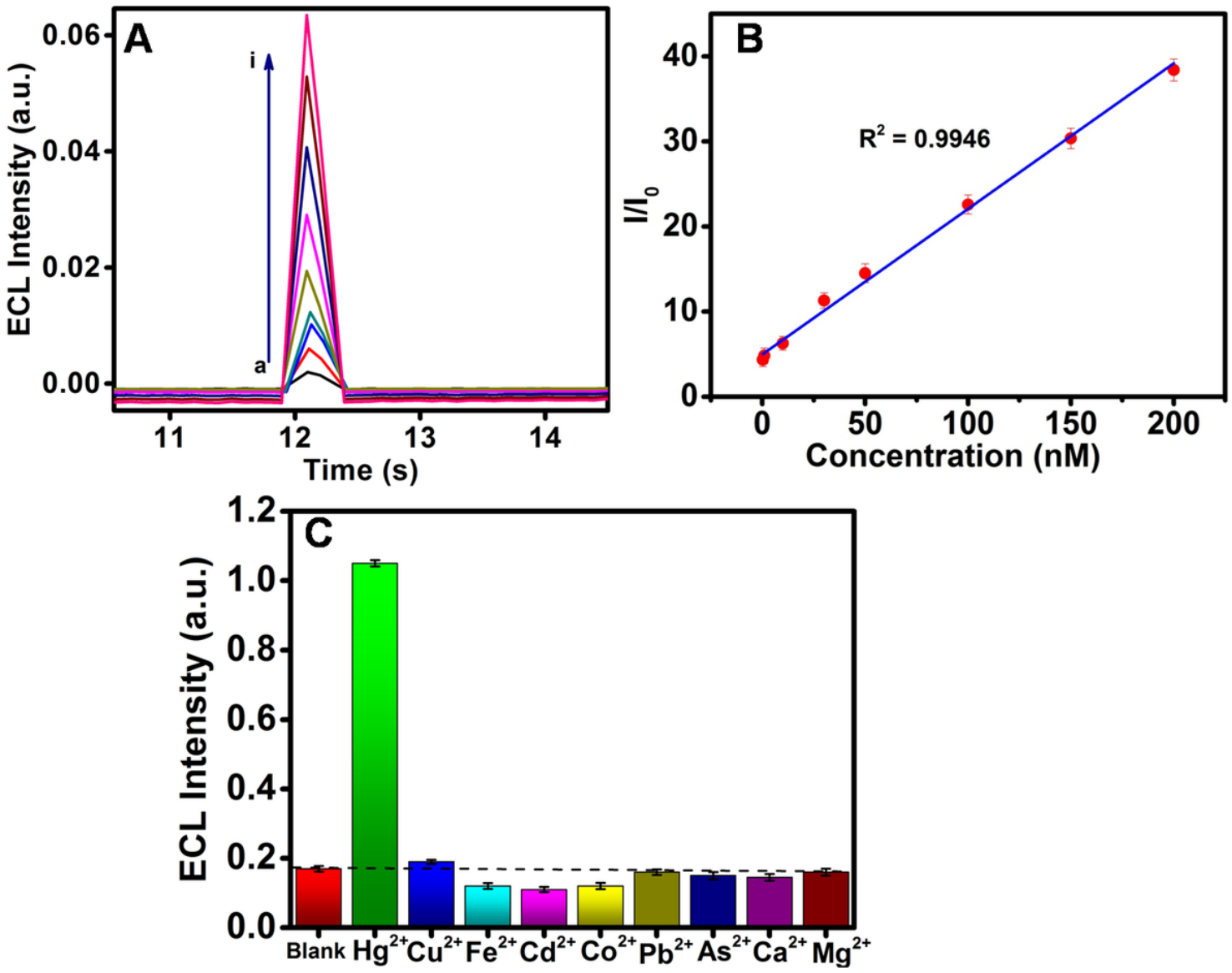

Figure 5

ECL intensity vs. time curves of (PL-Au)nano/GCE (A) and ECL spectrum (B) in O2 saturated 0.1 M PBS (pH 7.4) at several pulse potentials such as 0 to 0.6 V (a), -0.3 to 0.6 V (b), -0.6 to 0.6 V (c) and -0.8 to 0.6 V (d).

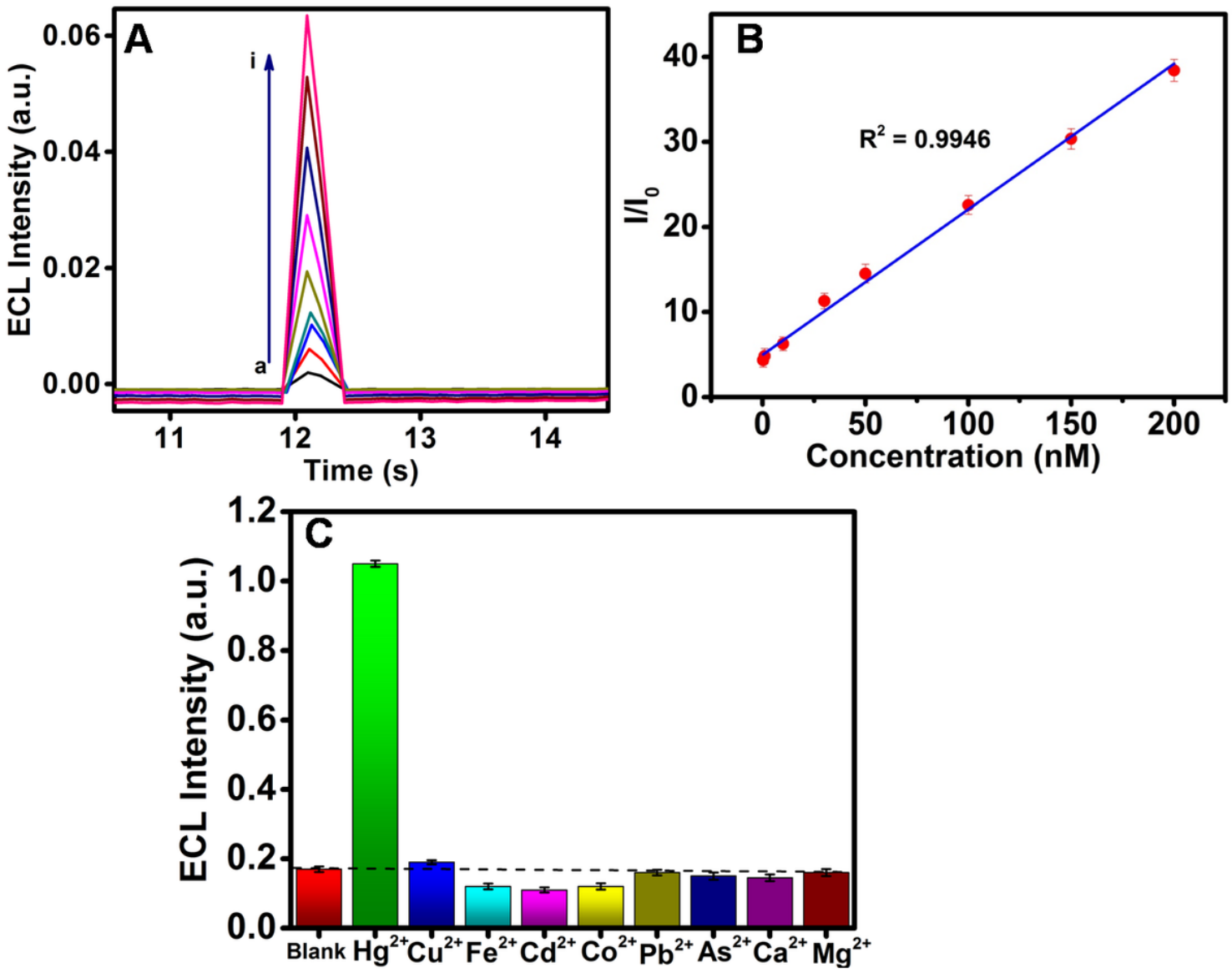

Figure 5

ECL intensity vs. time curves of (PL-Au)nano/GCE (A) and ECL spectrum (B) in O2 saturated 0.1 M PBS (pH 7.4) at several pulse potentials such as 0 to 0.6 V (a), -0.3 to 0.6 V (b), -0.6 to 0.6 V (c) and -0.8 to 0.6 V (d).

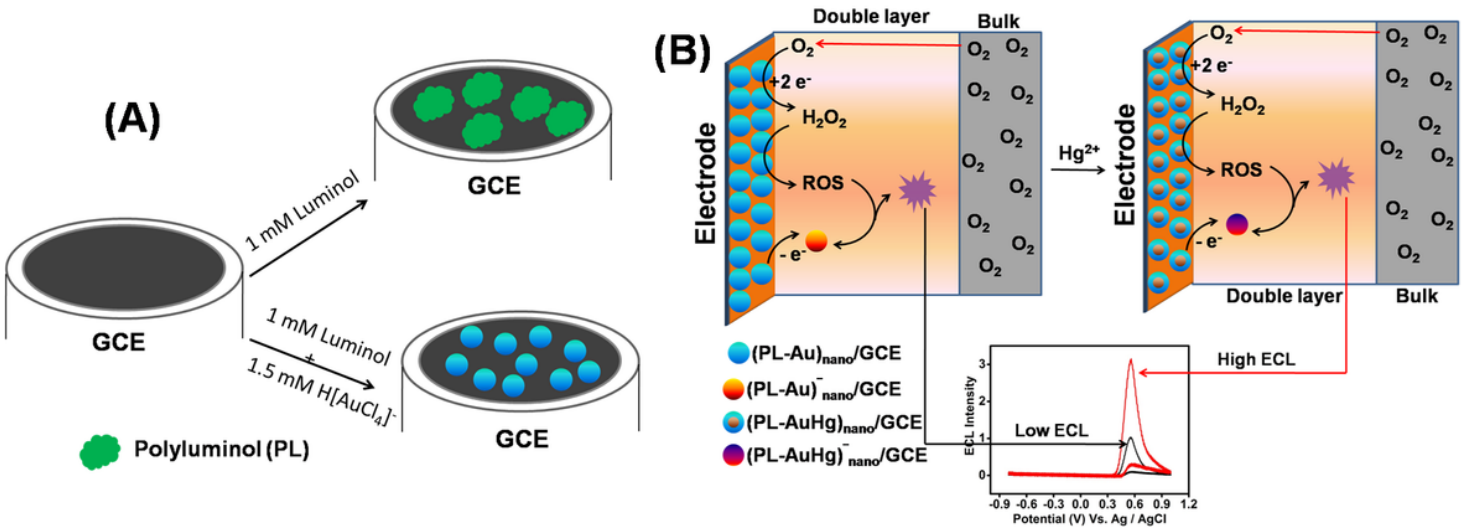

Figure 6

Schematic illustration of PL/GCE and (PL-Au)nano/GCE preparation (A) and ECL mechanism of (PL-Au)nano/GCE before and after Hg2+ addition (B).

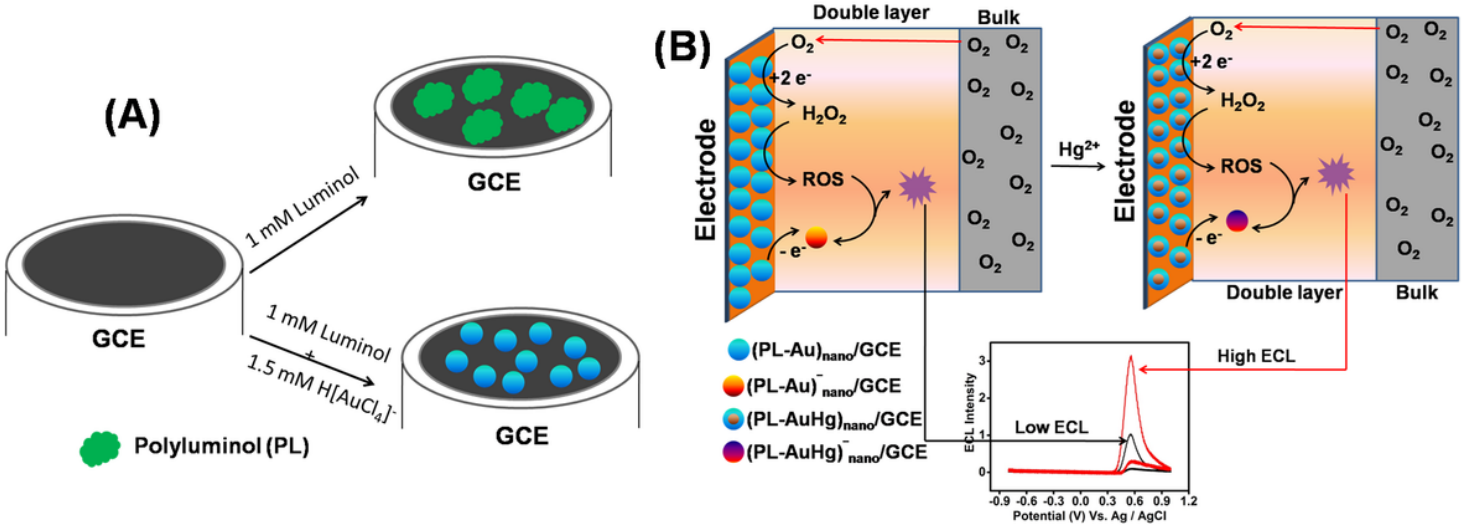

Figure 6

Schematic illustration of PL/GCE and (PL-Au)nano/GCE preparation (A) and ECL mechanism of (PL-Au)nano/GCE before and after Hg2+ addition (B).

Supplementary Files

This is a list of supplementary files associated with this preprint. Click to download.

- supportingfile.doc
- supportingfile.doc